lation and accumulation of cytoplasmic β-catenin. Our findings that β-catenin signaling can regulate the decisions of neural precursors to re-enter or exit the cell cycle lend support to the possibility that β-catenin signaling may mediate the loss of growth control when adherens junctions are disrupted.

It has been hypothesized that mutations in regulatory genes that control the decision of neural precursors to divide or differentiate can underlie the expansion of the precursor population without changing the thickness of the cortex (*5*, *11*). Here, we find that β-catenin activation can regulate the size of the neural precursor pool by influencing the decision to divide or differentiate, without increasing cell cycle rate, decreasing cell death, or grossly altering neuronal differentiation. Larger brains can be generated in different ways as well. For example, reduction of programmed cell death by targeted mutation of Caspase 9 causes severe brain malformations characterized by cerebral enlargement, ectopic growth, and thickening of the ventricular zone (*36*, *37*). In contrast, mice with targeted deletions of the cell cycle regulator $p27^{kip1}$ have increased body size and uniformly enlarged brains with virtually no anatomic abnormalities other than increased cell number and cell density (*38–40*). Notably, cortical surface area was not disproportionately increased (*38*). In contrast, our findings suggest that subtle changes in the expansion or maintenance of the neural precursor population result in horizontal expansion of the surface area of the developing cerebral cortex without increases in cortical thickness (*41*). Further understanding of how the decision to divide or differentiate is regulated by β-catenin will lend valuable insight into the mechanisms that underlie the disproportionate growth of the cerebral cortex in higher mammals.

References and Notes

1. B. L. Finlay, R. B. Darlington, *Science* **268**, 1578 (1995).
2. R. A. Barton, P. H. Harvey, *Nature* **405**, 1055 (2000).
3. D. A. Clark, P. P. Mitra, S. S. Wang, *Nature* **411**, 189 (2001).
4. V. S. Caviness Jr., T. Takahashi, R. S. Nowakowski, *Trends Neurosci.* **18**, 379 (1995).
5. P. Rakic, *Trends Neurosci.* **18**, 383 (1995).
6. H. Elias, D. Schwartz, *Science* **166**, 111 (1969).
7. H. Haug, *Am. J. Anat.* **180**, 126 (1987).
8. P. Rakic, *Science* **241**, 170 (1988).
9. V. B. Mountcastle, *Brain* **120**, 701 (1997).
10. Although the pyramidal neurons comprising the majority of cerebral cortical neurons appear to be generated in an approximately columnar arrangement, not all cortical neurons are derived from cortical ventricular zone progenitors, because the majority of cortical inhibitory interneurons are generated outside the cerebral cortex (*42*).
11. V. J. Caviness, T. Takahashi, R. S. Nowakowski, *Trends Neurosci.* **18**, 379 (1995).
12. R. T. Cox, C. Kirkpatrick, M. Leifer, *J. Cell Biol.* **134**, 133 (1996).
13. M. Peifer, P. Polakis, *Science* **287**, 1606 (2000).
14. B. A. Parr, M. J. Shea, G. Vassileva, A. P. McMahon, *Development* **119**, 247 (1993).
15. M. Oosterwegel *et al.*, *Development* **118**, 439 (1993).
16. E. A. Cho, G. R. Dressler, *Mech. Dev.* **77**, 9 (1998).
17. R. T. Moon, J. D. Brown, M. Torres, *Trends Genet.* **13**, 157 (1997).
18. A. P. McMahon, A. Bradley, *Cell* **62**, 1073 (1990).
19. S. M. Lee, S. Tole, E. Grove, A. P. McMahon, *Development* **127**, 457 (2000).
20. J. Galceran, E. M. Miyashita-Lin, E. Devaney, J. L. Rubenstein, R. Grosschedl, *Development* **127**, 469 (2000).
21. V. Brault *et al.*, *Development* **128**, 1253 (2001).
22. H. Huang *et al.*, *Am. J. Pathol.* **156**, 433 (2000).
23. S. Butz, L. Larue, *Cell Adhes. Commun.* **3**, 337 (1995).
24. H. Clevers, M. van de Wetering, *Trends Genet.* **13**, 485 (1997).
25. A. I. Barth, A. L. Pollack, Y. Altschuler, K. E. Mostov, W. J. Nelson, *J. Cell Biol.* **136**, 693 (1997).
26. P. J. Yaworsky, C. Kappen, *Dev. Biol.* **205**, 309 (1999).
27. Although the gyral convolutions of the adult human cortex also span all cortical layers, the ventricular surfaces remain relatively smooth, contrasting with the convoluted ventricular surfaces of β-catenin–transgenic animals. Despite this difference, sections through developing human brains show that the neural progenitor population in humans, like that of β-catenin–transgenic animals, consists of a thin, horizontally expansive epithelial sheet. Relative differences in the degree of mismatch between cortical surface area to skull volume may determine when cortical folding occurs and whether the resulting folding affects the entire cortical thickness.
28. T. Ohtsuka, M. Sakamoto, F. Guillemot, R. Kageyama, *J. Biol. Chem.* **276**, 30467 (2001).
29. T. Ohtsuka *et al.*, *Embo J.* **18**, 2196 (1999).
30. T. Scholzen, J. Gerdes, *J. Cell Physiol.* **182**, 311 (2000).
31. N. Kee, S. Sivalingam, R. Boonstra, J. M. Wojtowicz, *J. Neurosci. Methods* **115**, 97 (2002).
32. C. V. DiSalvo, D. Zhang, J. W. Jacobberger, *Cell Prolif.* **28**, 511 (1995).
33. C. Y. Kuan, K. A. Roth, R. A. Flavell, P. Rakic, *Trends Neurosci.* **23**, 291 (2000).
34. T. Takahashi, R. S. Nowakowski, V. S. Caviness Jr., *J. Neurosci.* **16**, 6183 (1996).
35. D. Bilder, M. Li, N. Perrimon, *Science* **289**, 113 (2000).
36. K. Kuida *et al.*, *Cell* **94**, 325 (1998).
37. R. Hakem *et al.*, *Cell* **94**, 339 (1998).
38. M. L. Fero *et al.*, *Cell* **85**, 733 (1996).
39. H. Kiyokawa *et al.*, *Cell* **85**, 721 (1996).
40. K. Nakayama *et al.*, *Cell* **85**, 707 (1996).
41. For a discussion of potential mechanical forces that lead to cortical folds, see D. C. Van Essen, *Nature* **385**, 313 (1997).

42. S. A. Anderson, O. Marin, C. Horn, K. Jennings, J. L. Rubenstein, *Development* **128**, 353 (2001).
43. M. van de Wetering *et al.*, *Cell* **88**, 789 (1997).
44. Supported by National Institute of Neurological Disorders and Stroke grant R01NS32457 (C.W.). A. C. was a Howard Hughes Medical Institute Physician Postdoctoral Fellow. We thank A. Barth and W. J. Nelson, Stanford, for ΔN90β-catenin-kt3 DNA reagent; J. M. Hebert, A. Okada, and S. K. McConnell, Stanford, for nestin, enhanced green fluorescent protein (EGFP) constructs; M. van de Wetering, Utrecht, for pTOPFLASH and pFOPFLASH reagent; E. Fuchs, University of Chicago, for hLef1 reagent; R. Kageyama for *Hes1* and *Hes5* in situ probes; R. R. Ratan, Harvard, for the luminometer; U. Berger for in situs; L. Du, T. Thompson, and S. White for technical assistance; P. Webster, Zymogenetics, for transgenic construct design; and X. He and members of the Walsh lab for comments on the manuscript.

Supporting Online Material

www.sciencemag.org/cgi/content/full/297/5580/365/DC1
Materials and Methods
References and Notes
Fig. S1

21 May 2002; accepted 25 June 2002

Nonresonant Multiple Spin Echoes

Thilo M. Brill,* Seungoh Ryu, Richard Gaylor, Jacques Jundt, Douglas D. Griffin, Yi-Qiao Song, Pabitra N. Sen, Martin D. Hürlimann

Nonresonant manipulation of nuclear spins can probe large volumes of sample situated in inhomogeneous fields outside a magnet, a geometry suitable for mobile sensors for the inspection of roads, buildings, and geological formations. However, the interference by Earth's magnetic field causes rapid decay of the signal within a few milliseconds for protons and is detrimental to this method. Here we describe a technique to suppress the effects of Earth's field by using adiabatic rotations and sudden switching of the applied fields. We observed hundreds of spin echo signals lasting for more than 600 milliseconds and accurately measured the relaxation times of a liquid sample.

Conventional nuclear magnetic resonance (NMR) experiments are almost always carried out by manipulating nuclear spins using radio frequency (rf) pulses at the spin Larmor frequency $\omega = \gamma B$, where γ is the gyromagnetic ratio and B is the magnitude of the magnetic field. Such resonant NMR experiments allow the imaging of spins in materials and the characterization of spin interactions, enabling applications extending to materials such as soft condensed matter (*1*), plants (*2*), food products (*3*), cement and concrete (*4*), and geological materials (*5*, *6*). The field applications are the motivation for several recent developments in ex situ NMR (*7–10*), where a mobile NMR detector is used to examine the sample outside the NMR magnet. However, as a result of the geometry of such mobile tools, the applied magnetic fields exhibit large inhomogeneities, and all resonant techniques will result in small sensitive volumes where the resonance condition is satisfied. Composite (*11*) and adiabatic (*12*) pulses may be used to expand the excitation bandwidth to a limited extent at the expense of higher irradiation power.

Alternatively, spins can be manipulated

by suddenly switching the direction of the magnetic field (*13*, *14*), and the formation of echoes has been demonstrated (*15*) using sudden field reversal. These nonresonant techniques can greatly expand the detection volume, because they excite nuclear magnetization with an efficiency independent of the Larmor frequency. However, background fields such as Earth's field, which are difficult to shield in ex situ applications, lead to an imperfect field inversion. The presence of inhomogeneous applied fields results in a rapid echo decay with a time constant on the order of a few Larmor periods of the background field (that is, milliseconds for protons in the presence of Earth's field).

We demonstrate here a technique that overcomes the detrimental effects of the background fields and can produce hundreds of echoes by maintaining the spin coherence for time periods up to seconds, limited by the intrinsic relaxation time. The essence of our approach is the use of combined sudden switching and adiabatic rotations (CSAR) of the applied fields (*16*). To demonstrate the basic principle of CSAR, we used the experimental setup shown in Fig. 1 with two sets of coils (labeled A and B) that can be independently energized and can produce magnetic fields of modest homogeneity (25%) that are mostly orthogonal to each other within the sample volume. Induced oscillating magnetization is detected with a third set of detection coils, orthogonal to the other two coils to minimize mutual inductance.

Although the basic nonresonant sequence in Fig. 1B can generate multiple echoes (Fig. 1C), the amplitudes decay rapidly (within 7 ms) for our setup with water protons. In contrast, the early echo signals from a CSAR sequence (Fig. 1, D and E) demonstrate that CSAR sequences can overcome the enhanced echo decay caused by Earth's field.

Both sequences begin with an initial segment where the field B_A is applied to polarize the nuclear spins. This field is then abruptly turned off, and immediately the field B_B, mainly orthogonal to B_A, is turned on, also nonadiabatically (*13*, *17*–*19*). This segment may be likened to the preparatory 90° pulse in conventional NMR but is effective for a much broader range of fields. Next, we analyze the rapid echo decay of the sequence in Fig. 1B caused by the effects of background fields. During the free precession period that follows the 90° pulse (Fig. 1B), spins at position $\vec{r}$ acquire a phase $\phi(\vec{r}) \approx \gamma t[B_B(\vec{r}) + B_e\cos\alpha(\vec{r})]$ where $\alpha(\vec{r})$ is the angle between $B_B(\vec{r})$ and the background field B_e, assumed to be much smaller than B_B. A reversal of B_B after a time t (Fig. 1B) will cancel the $B_B(\vec{r})$ contribution to ϕ at the nominal echo time $2t$ but will leave a residual phase ($\delta\phi$) of $2\gamma B_e t\cdot\cos\alpha$. Inhomogeneity in B_B and the resulting spatial distribution of α lead to a nonzero second moment of the residual phase and thus to an echo decay at a rate of $\gamma B_e \sqrt{<\cos\alpha^2>}$ $- <\cos\alpha>^2/2$, where $< \ldots >$ signifies spatial averaging. The rapid signal decay in Fig. 1C is consistent with the 15° range of α over the sample in our setup. This decay mechanism is a first-order effect independent of B_B; that is, it cannot be overcome by enlarging the switching fields.

CSAR-based sequences are designed to expose the spins to the same progression of local fields before and after the field reversals in order to cancel $\delta\phi$ everywhere, similar to spin echoes in resonant NMR (*20*, *21*). The CSAR sequence shown in Fig. 1D is designed to refocus every second echo. After a short period of free precession under B_B, the applied field is adiabatically rotated by a nominal angle of 90° by application of a slow sinusoidal variation of the respective strengths of the currents in the coils *A* and *B*. The rate of this adiabatic rotation, Ω, satisfies $\Omega << \gamma B_A$ and $\Omega << \gamma B_B$ so that the magnetization remains orthogonal to the instantaneous local field. Then the field is inverted nonadiabatically ($B_A \rightarrow -B_A$) and subsequently rotated adiabatically back to the original direction. We call this sequence (segments 1 through 4) a CSAR refocusing sequence, which includes the adiabatic (1 to 2 and 3 to 4) and nonadiabatic (2 to 3) segments (Fig. 1D).

Without a background field, a single refocusing sequence already leads to an echo formation. However, in the presence of a background field, $\delta\phi$ has both dynamical and geometrical contributions (*22*, *23*) that do not vanish, and no echo forms after segments

Schlumberger-Doll Research, 36 Old Quarry Road, Ridgefield, CT 06877, USA.

*To whom correspondence should be addressed. E-mail: brill2@slb.com

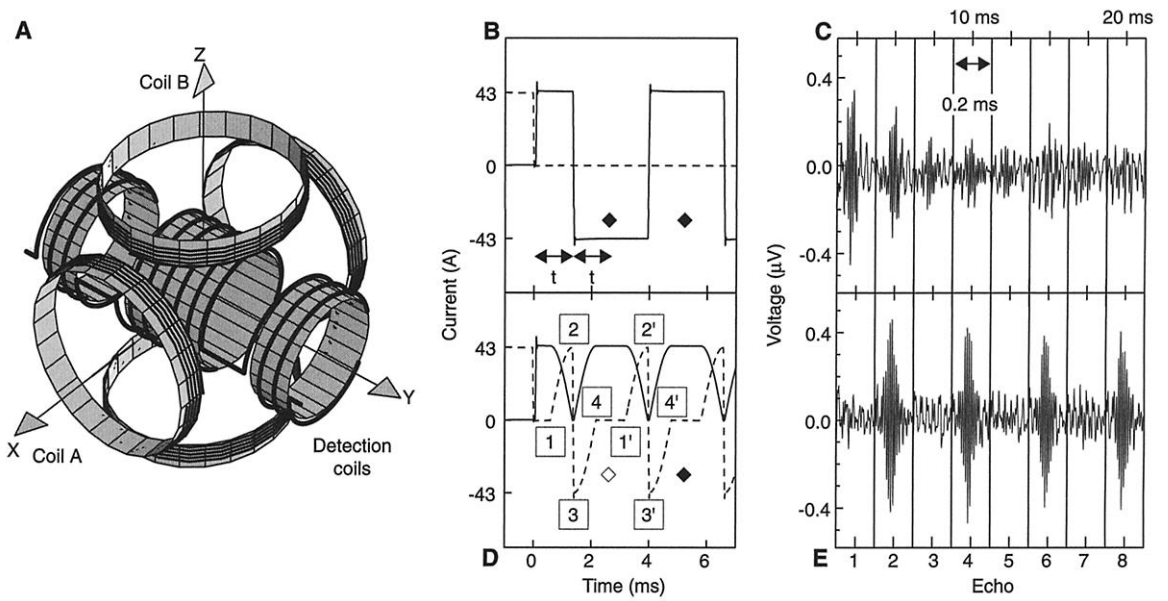

Fig. 1. (**A**) The orientation of the two orthogonal Helmholtz coils (14 cm in diameter), positioned so that Earth's field lies along the axis of coil B. A current of 43 A generates a field of 2.14 mT at the center of a given pair of coils. The sample of $NiCl_2$-doped water with a T_1 = T_2 = 510 ms fills the cylindrical space, 7.6 cm in diameter and 8.3 cm in length, inside the central coil of the second-order gradient coil receiver. Two nonresonant NMR sequences are shown: (**B**) and (**C**), the basic nonresonant sequence; and (**D**) and (**E**), the CSAR sequence. [(B) and (D)] The dashed lines show the time dependence of current I_A through coil A, and the solid lines show the current I_B through coil B. [(C) and (E)] The resulting oscillatory voltage signals measured by the detection coil in 0.2-ms-long acquisition windows centered around the nominal echo times indicated by diamonds in (B) and (D) with an echo spacing of 2.5 ms. Each trace is the result of 1000 signal averages. The average frequency of the fast signal oscillations at 90 kHz coincides with the average Larmor frequency applied across the sample. The initial echo amplitude is consistent with the expected signal from the whole sample, and the measured width of the echoes is in agreement with the root mean square B_B inhomogeneity of 25% and the detection bandwidth. The first few odd echoes in (D) and (E) (open diamond) are in the noise level.

1 through 4. Nevertheless, the magnitude of this extra phase is identical from interval to interval because the local field trajectories are repeated. After every second CSAR refocusing sequence, the echo recovers its full amplitude (Fig. 1E): The phase accumulation in segments 1 to 2 and 3 to 4 is canceled by the phase accumulation during 1′ to 2′ and 3′ to 4′, because the sense of precession is reversed during the field reversal in segment 2 to 3 (2′to 3′). This compensation is independent of the inhomogeneity of the applied or background field, and it also compensates for any dc offsets in the currents applied to the coils. It only relies on the adiabaticity during the field rotations and on sufficiently sudden field reversals.

Because a single CSAR refocusing sequence in this implementation does not cancel $\delta\phi$, the amplitudes of odd echoes are initially at the noise level. At later echoes, Fig. 2 shows a more complicated behavior. The even and odd echo amplitudes exhibit a slow oscillation with a period of many echoes. The decay of echo amplitudes can be separated into two components. A fraction equal to about 50% of the initial even echo amplitude decays exponentially with the intrinsic relaxation time (T_2) of the sample, T_2 = 510 ms. Superimposed on this component is a second component of about equal amplitude with an odd-even dependence that is modulated with a Bessel-like function. The period and decay time of this modulation are determined by imperfections of the sudden field reversal and deviations from adiabaticity during the slow field rotation. We have found through experiments and numerical simulations that the dominant imperfection is the finite duration of the field reversals (nominally 75 T/s in the example shown in Fig. 1D).

The presence of the first component enables the accurate determination of long transverse relaxation times. In addition, the long echo train allows a substantial improvement of the signal-to-noise ratio that benefits experiments to determine T_1 and imaging. We have used this technique to perform T_1 measurements by varying the initial polarization time.

To better understand this sequence and to identify other sequences of repetitive spin manipulations suitable to measure long relaxation times, we used an approach based on the effective rotation axis method (*9*, *24*). This method describes the echo-to-echo propagator as a net rotation and concentrates on the magnetization component along the axis of this net rotation. This magnetization component is invariant from echo to echo; that is, perfectly refocused. Next, we describe how the effective rotation axis method can be used to design improved CSAR sequences.

For the CSAR sequence shown in Fig. 1D, with the limit of fully adiabatic rotations and perfect field reversals, a single refocusing sequence is described by a π rotation around an axis $\hat{n}$ in a plane perpendicular to B_B. The direction of $\hat{n}$ within this plane is determined by the size of $\delta\phi$ because of the background fields. In sufficiently inhomogeneous fields, $\hat{n}$ is uniformly distributed within this plane. Because the initial magnetization after the polarization is pointing predominantly along the $\hat{x}$ axis, a fraction of $\langle(\hat{n}\cdot\hat{x})^2\rangle \simeq 1/2$ of the magnetization is refocused along the x axis. This contribution decays with T_2. The other half of the initial magnetization oscillates around the net rotation axis, giving rise to the odd-even echo modulation.

With imperfections in the adiabatic rotations or field reversals, the angle of the net rotations will deviate from π. This deviation does not affect the component that is colinear with $\hat{n}$ decaying with T_2. But for the other component, the accumulated deviations from the nominal π rotations lead to a Bessel function–like oscillatory decay after averaging over the sample volume, as observed experimentally (Fig. 2).

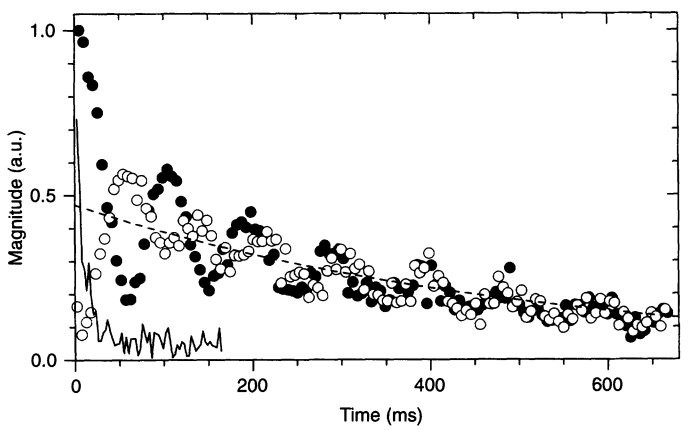

Fig. 2. Magnitudes of multiple spin echo amplitudes versus time for two different nonresonant refocusing sequences. The solid and open symbols show the magnitudes of the first 256 echoes obtained by the CSAR sequence of Fig. 1D for odd and even echo numbers, respectively. The average decay closely follows the exponential decay of the $NiCl_2$-doped water with a T_2 = 510 ms, as indicated by the dashed line. Bessel function–like oscillations are superimposed on the exponential decay of the echo magnitude (see also the expanded scale of Fig. 3A). In contrast, the solid line shows the results for the basic nonresonant sequence (Fig. 1B) displaying rapid signal decay. a.u., arbitrary units.

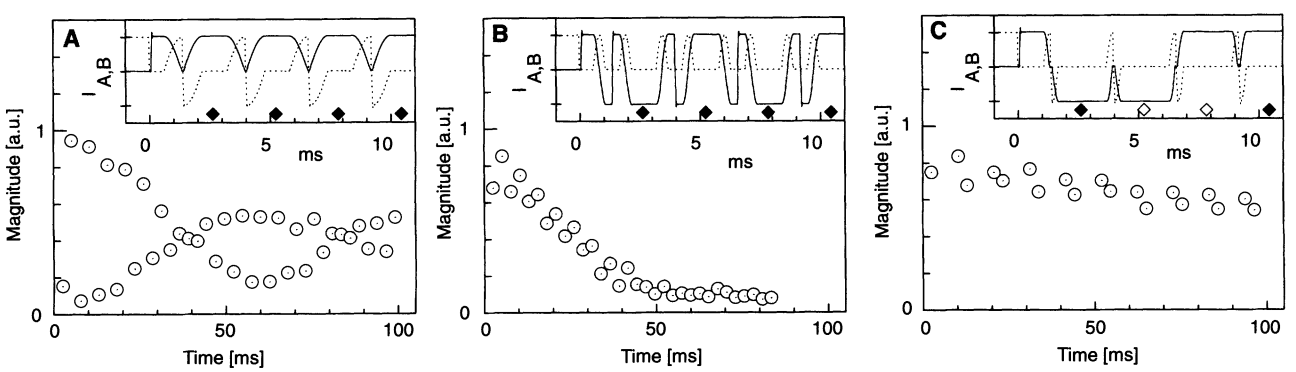

Fig. 3. Comparison of multiple spin echo magnitudes versus time for different CSAR sequences. The sequences are shown as insets with the currents I_A (dotted line) and I_B (solid line) through coils A and B, respectively, as described in Fig. 1. The echo times of the displayed amplitudes are marked by diamonds. The echo spacings are 2.6 ms in all cases. (**A**) The results for the sequence of Fig. 1D, with CSAR refocusing sequences involving sudden field reversals sandwiched by 90° adiabatic rotations. There is a strong even-odd echo modulation. (**B**) Sudden field reversals sandwiched by 180° adiabatic rotations. Sequence (**C**) is similar to sequence (A), except that the senses of the adiabatic rotations are changed to better compensate for imperfections. The echo amplitudes for the positions indicated by open diamonds in the inset of (C) are in the noise level and have been omitted.

Motivated by our analysis, we have explored other implementations of the CSAR concept. The echo-to-echo propagator of a single refocusing sequence shown in Fig. 3B is to first order a rotation by 2π rather than π. Therefore, we expect refocusing of both even and odd echoes. This refocusing was seen experimentally with a slight even-odd modulation. The sequence consists of two subcycles, each composed of a nonadiabatic reversal of field B_B sandwiched between two adiabatic 180° rotations. Although the sequence is superior to the basic nonresonant sequence (Fig. 1B), the later echoes show an enhanced decay because the observed magnetization comes mainly from components perpendicular to $\hat{n}$. Finite reversal times lead to deviations of the rotation angle from the perfect 2π rotations that accumulate rapidly over several refocusing cycles.

These results suggest that the enhanced decay can be reduced by the use of a technique inspired by the broadband inversion techniques in resonant NMR, which use supercycles of rf phases (*25*, *26*) to compensate progressively for higher-order imperfections and inhomogeneities of rf and static fields. Instead of controlling the phase of rf pulses, we have the ability in nonresonant NMR to change the sense of the adiabatic rotations. Such a technique has been implemented in Fig. 3C. The sequence is based on the refocusing unit of the sequence in Fig. 3A and incorporates a four-unit supercycle of different senses of adiabatic rotation. The results show large amplitudes for echoes 4, 8, 12, and so on and slightly smaller ones for echoes 1, 5, 9, and so on, with a much smaller initial decay rate than the other sequences. The perturbative nature of the average Hamiltonian theory is particularly useful for the design of sequences with superior performance at early echoes (*25*, *26*). However, for increased echo numbers, the observed decay rate is still much higher than the intrinsic relaxation rate, and an approach based on the effective rotation-axis method is better suited to find sequences for T_2 measurements.

The nonresonant NMR methods described here require fast switching of applied fields that are sufficiently large, as compared to the background field, to achieve field reversal. These factors limit the sensitive volume achievable in practical ex situ applications, where fields weaken with distance. Although it appears to be impractical to employ the rather low magnetic fields of nonresonant NMR to perform chemical shift analyses, the CSAR sequences can be extended to include segments of pulsed-field gradients to perform imaging in a manner similar to conventional magnetic resonance imaging. The technique has further potential applications in multinuclei detection.

References and Notes

1. R. Muthupillai *et al.*, *Science* **269**, 1854 (1995).
2. C. F. Jenner, Y. Xia, C. D. Eccles, P. T. Callaghan, *Nature* **336**, 399 (1988).
3. M. J. McCarthy, *Magnetic Resonance Imaging in Foods* (Chapman & Hall, New York, 1994).
4. W. P. Halperin, F. D'Orazio, S. Bhattacharja, J. C. Tarczon, in *Molecular Dynamics in Restricted Geometries*, J. Klafter, J. Drake, Eds. (Wiley, New York, 1989), pp. 311–350.
5. J. F. Stebbins, I. Farnan, *Science* **245**, 257 (1989).
6. Y.-Q. Song, S. Ryu, P. N. Sen, *Nature* **406**, 178 (2000).
7. R. L. Kleinberg, "Well logging," in *Encyclopedia of Nuclear Magnetic Resonance* (Wiley, Chichester, UK, 1996), vol. 8, pp. 4960–4969.
8. G. Eidmann, R. Savelsberg, P. Blümler, B. Blümich, *J. Magn. Reson. A* **122**, 104 (1996).
9. M. D. Hürlimann, D. D. Griffin, *J. Magn. Reson.* **143**, 120 (2000).
10. C. A. Meriles, D. Sakellariou, H. Heise, A. J. Moulé, A. Pines, *Science* **293**, 82 (2001).
11. M. H. Levitt, "Composite pulses," in *Encyclopedia of Nuclear Magnetic Resonance* (Wiley, Chichester, UK, 1996), vol. 2, pp. 1396–1411.
12. M. Garwood, L. DelaBarre, *J. Magn. Reson.* **153**, 155 (2001).
13. M. E. Packard, R. Varian, *Phys. Rev.* **93**, 941 (1954).
14. A. Abragam, *Principles of Nuclear Magnetism* (Clarendon, Oxford, UK, 1978).
15. R. McDermott *et al.*, *Science* **295**, 2247 (2002).
16. M. D. Hürlimann, Y.-Q. Song, S. Ryu, P. N. Sen, U.S. Patent 6,133,735 (October 2000).
17. B. F. Melton, V. L. Pollack, *Rev. Sci. Instrum.* **42**, 769 (1971).
18. R. N. Chandler, W. E. Kenyon, C. E. Morriss, *Transactions of the 28th Annual SPWLA Logging Symposium*, London, England, 29 June to 2 July, 1987, vol. 1, (SPWLA, Houston, TX, 1987), pp. C1–C25.
19. D. J. Sloop, T.-S. Lin, J. J. H. Ackerman, *J. Magn. Reson.* **139**, 60 (1999).
20. E. L. Hahn, *Phys. Rev.* **80**, 580 (1950).
21. I. Solomon, *Phys. Rev. Lett.* **2**, 301 (1959).
22. M. V. Berry, *Proc. R. Soc. London Ser. A* **392**, 45 (1984).
23. J. W. Zwanziger, M. Koenig, A. Pines, *Annu. Rev. Phys. Chem.* **41**, 601 (1990).
24. M. D. Hürlimann, *J. Magn. Reson.* **152**, 109 (2001).
25. M. H. Levitt, R. Freeman, T. Frenkiel, *Adv. Magn. Reson.* **11**, 47 (1983).
26. R. Tycko, *Phys. Rev. Lett.* **51**, 775 (1983).

26 March 2002; accepted 15 May 2002

Direct Measurement of the Reaction Front in Chemically Amplified Photoresists

Eric K. Lin,[1]* Christopher L. Soles,[1] Dario L. Goldfarb,[3] Brian C. Trinque,[4] Sean D. Burns,[4] Ronald L. Jones,[1] Joseph L. Lenhart,[1] Marie Angelopoulos,[3] C. Grant Willson,[4] Sushil K. Satija,[2] Wen-li Wu[1]

The continuing drive by the semiconductor industry to fabricate smaller structures using photolithography will soon require dimensional control at length scales comparable to the size of the polymeric molecules in the materials used to pattern them. The current technology, chemically amplified photoresists, uses a complex reaction-diffusion process to delineate patterned areas with high spatial resolution. However, nanometer-level control of this critical process is limited by the lack of direct measurements of the reaction front. We demonstrate the use of x-ray and neutron reflectometry as a general method to measure the spatial evolution of the reaction-diffusion process with nanometer resolution. Measuring compositional profiles, provided by deuterium-labeled reactant groups for neutron scattering contrast, we show that the reaction front within the material is broad rather than sharply defined and the compositional profile is altered during development. Measuring the density profile, we directly correlate the developed film structure with that of the reaction front.

The tremendous device performance increases by the semiconductor industry have been driven by the successful development of materials and tools for the high-volume fabrication of smaller device structures with photolithography. By 2003, the semiconductor industry predicts that structures with sub–100-nm critical dimensions will be needed (*1*), but many difficult materials challenges remain. The critical dimension must be controlled over 2 to 5 nm length scales, which is comparable to the characteristic size of the polymeric molecules in the photoresists used to pattern the features (*2*). Furthermore, thinner photoresist films are required because of increasing optical absorption with decreasing imaging wavelengths. Thinner photoresist films and the production of nanoscale structures can involve changes in key photoresist properties from those of the bulk material (*3*–*6*). Quantitative measurements of material

[1]Polymers Division and [2]Center for Neutron Research, National Institute of Standards and Technology, Gaithersburg, MD 20899–8541, USA. [3]IBM T. J. Watson Research Center, Yorktown Heights, NY 10598, USA. [4]Departments of Chemistry and Chemical Engineering, University of Texas at Austin, Austin, TX 78712, USA.

*To whom correspondence should be addressed. E-mail: eric.lin@nist.gov